Experimental Measurements of the Flow in a Scramjet Inlet at Mach 4

William J. Yanta,* Arnold S. Collier,† W. Charles Spring III,‡ and Christopher F. Boyd§
Naval Surface Warfare Center, Silver Spring, Maryland 20903
and
J. Craig McArthur¶
North Carolina State University, Raleigh, North Carolina 27695

Wind-tunnel measurements have been carried out in a scramjet inlet model at a freestream Mach number of 4.00. Measurements included velocity profiles using a two-dimensional laser Doppler velocimeter (LDV), Mach number surveys, skin friction measurements with Preston probes, wall static pressure distributions, density profiles with a laser holographic interferometer, and qualitative shadowgraph photography. The effect of boundary-layer bleed on the viscous flow entering the inlet was also investigated. It was determined that bleeding off the boundary layer increased the inlet efficiency substantially.

Nomenclature

c_f	= coefficient of friction
M	= Mach number
P	= pressure
P_0'	= pitot pressure
$\bar{P}$	= P_0'/P_0
S	= surface distance
T	= temperature
U	= velocity component parallel to surface
$<U'>$	= rms of turbulent fluctuations
V	= velocity component perpendicular to surface
x,y,z	= Cartesian coordinates
γ	= ratio of specific heats
ρ	= gas density
τ	= shear stress

Subscripts

cl	= centerline
max	= maximum
0	= tunnel supply conditions
w	= wall
∞	= freestream

Introduction

THE use of ramjets/scramjets as a viable propulsion method has seen a resurgence in the last several years. One of the important aspects of the design of a ramjet/scramjet system is the inlet. In general, previous investigations of scramjet inlets have been limited to global engineering measurements of air capture, exit flow properties, and pressure recovery.[1] There are several references that describe experiments in which the details of the flow in and around inlets have been investigated. For example, some investigators have characterized the flow leading up to the inlet.[2-6] Others have carried out experiments in ducts with either circular or square cross sections.[7-9] In these experiments, the supersonic flow developing in a duct was uniform in the entrance region. The interaction of the developing boundary layer with the internal flow was of primary interest. Sajben and co-workers have carried out numerous experiments in a supersonic diffuser type of device that simulates a ramjet type of inlet.[10-12] There is a limited amount of experimental data that describes the internal fluid mechanics in a scramjet inlet in which the flow has undergone some precompression.[13-15]

Because current computational fluid dynamics (CFD) methods have reached a high degree of sophistication and are capable of computing the flowfields in and around very complex configurations,[16] there has developed a real need for comprehensive experiments to both understand the flow phenomena that occurs in these flows and to give computationalists the opportunity to assess the validity and/or accuracy of the CFD computations. Since these codes can give very detailed information about many flow variables, this has challenged the experimentalist to also obtain as much information as possible from an experiment. That was the spirit in which this experiment was carried out.

The purpose of this experiment was to investigate, in considerable detail, the flowfield that occurs in a generic, two-dimensional scramjet inlet. The data obtained include laser Doppler velocimeter (LDV) measurements of the mean and fluctuating velocities, skin friction data taken with Preston probes, Mach number surveys at a number of stations in the inlet, wall static pressure distributions along the inlet walls, shadowgraph photos, and density distributions obtained from laser holographic interferometry (LHI). In addition, the boundary layer being ingested into the inlet was controlled by applying suction, and all the measurements were made with and without boundary-layer bleed. Because of the relatively low Reynolds number, the boundary layer was also tripped for some cases.

The Model

A schematic diagram and a table of the coordinates of the scramjet inlet model used in these experiments are shown in Fig. 1 and Table 1, respectively. The inlet was an inward-turning scoop type. The forebody wedge (10-deg wedge angle) was used to give some precompression to the flow entering the inlet. The leading edge of the inlet cowl was a 10-deg wedge,

Presented as Paper 88-0271 at the AIAA 26th Aerospace Sciences Meeting, Reno, NV, Jan. 11-14, 1988; received July 7, 1988; revision received Aug. 16, 1989.

*Chief Technologist, Aerodynamics Branch. Associate Fellow AIAA.
†Aerospace Engineer, Aerodynamics Branch. Member AIAA.
‡Photographic Technologist, Graphics and Photographics Section.
§Aerospace Engineer, Aerodynamics Branch. Member AIAA.
¶Graduate Student, Dept. of Mechanical and Aerospace Engineering. Student Member AIAA.

Table 1 Model coordinates[a]

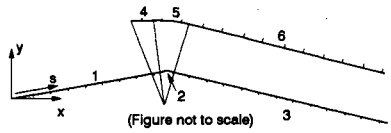

Section	Region of validity
1, straight line	
$y=0.1763x$	$0 \le x \le 13.5798$
[$y=0.1763x$]	[$0 \le x \le 34.4876$]
2, circular arc	
radius = 2.2547 [5.7269]	$13.5798 \le x \le 14.4734$
center at (13.9706, 0.1735)	[$34.4927 \le x \le 36.7624$]
[35.4853, 0.4407]	
3, straight line	
$y = -x \tan(13.0326 \text{ deg}) + 5.7216$	$14.4734 \le x \le 34.0000$
[$y = -x \tan(13.0326 \text{ deg}) + 14.5329$]	[$36.7624 \le x \le 86.3600$]
4, straight line	
$y = 3.6990$	$10.5175 \le x \le 11.6538$
[$y = 9.3955$]	[$26.7145 \le x \le 29.6007$]
5, isentropic compression focus point	
(14.7857, 1.9923)	$11.6538 \le x \le 13.4959$
[37.5557, 5.0604]	[$29.5986 \le x \le 34.2796$]

x	y
11.6538 [29.6007]	3.6990 [9.3955]
11.7612 [29.8734]	3.6985 [9.3942]
11.8660 [30.1396]	3.6970 [9.3904]
11.9682 [30.3992]	3.6946 [9.3843]
12.0680 [30.6527]	3.6913 [9.3759]
12.1653 [30.8686]	3.6871 [9.3652]
12.2602 [31.1409]	3.6822 [9.3528]
12.3527 [31.3759]	3.6764 [9.3381]
12.4430 [31.6052]	3.6699 [9.3215]
12.5310 [31.8287]	3.6627 [9.3033]
12.6169 [32.0469]	3.6548 [9.2832]
12.7007 [32.2598]	3.6468 [9.2629]
12.7823 [32.4670]	3.6371 [9.2382]
12.8620 [32.6695]	3.6274 [9.2136]
12.9397 [32.8668]	3.6171 [9.1874]
13.0154 [33.0591]	3.6063 [9.1600]
13.0893 [33.2468]	3.5951 [9.1316]
13.1614 [33.4300]	3.5833 [9.1016]
13.2316 [33.6083]	3.5711 [9.0706]
13.3002 [33.7825]	3.5585 [9.0386]
13.3671 [33.9524]	3.5454 [9.0053]
13.4323 [34.1180]	3.5320 [8.9713]
13.4959 [34.2796]	3.5183 [8.9365]

6, straight line	
$y = x \tan(12.7213 \text{ deg}) + 6.5650$	$13.5374 \le x \le 34.0000$
[$y = -x \tan(12.7213 \text{ deg}) + 16.6751$]	[$34.3850 \le x \le 86.3600$]

[a]Dimensions in inches, quantities in square brackets in cm.

which provided additional compression. This wedge was followed by an isentropic compression surface, which turned the flow 13 deg. The isentropic compression surface was designed to provide shock-free flow through the inlet at a freestream Mach number of 3. The oblique shock, which emanated from the 10-deg cowl wedge, struck the lower surface on the duct. This cowl shock was then canceled with a Prandtl-Meyer expansion of the lower surface. The isentropic compression surface was designed using centered-wave theory.[17] These compression waves were canceled by additional turning of the inner surface resulting (inviscidly) in a uniform flow with a Mach number of 2.09 entering the duct. The isentropic compression waves were focused, not on the inner surface, but on a point beneath the surface. This was done to weaken the resulting pressure gradients along the lower surface. Inlets are generally designed to compromise several flight conditions.

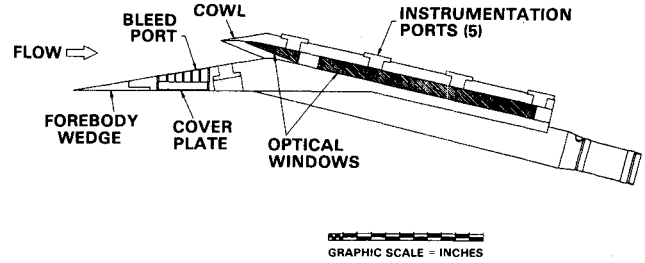

Fig. 1 Wind-tunnel model schematic.

The isentropic compression surface of this inlet was designed for a freestream Mach number of 3. The maximum air capture was designed for Mach 5. This was accomplished by having the shock from the model's leading edge impinge on the cowl leading edge.

After an inviscid design was determined, a boundary-layer calculation was made of the flow inside the duct. The displacement thickness was determined for the upper and lower surface only (the side wall boundary layers were not computed). The duct height was slightly divergent to compensate for the viscous displacement. Because the displacement thickness was nearly linear with duct length, it was assumed to be a linear increase to simplify fabrication. It should also be pointed out that rather than leaving a sharp corner on the lower surface where the Prandtl-Meyer expansion took place, a circular arc was used to connect the wedge surface to the duct. The duct width was 4.026 in. (10.23 cm) with a nominal height of 1 in. (25.4 mm). The cowl height was 1.813 in. (4.605 cm). The width of the forebody wedge was 16 in. (40.64 cm). The coordinates and an analytical description of the model surface are given in Table 1.

The flow underwent a total turning angle of 33 deg (10 deg upward on the wedge, 10 deg downward from the cowl wedge, and 13 deg through the isentropic compression) before entering the duct. The inlet was equipped with glass windows to provide access for the LDV and holographic interferometer. In addition, instrumentation ports in the duct wall provided a means of taking wall Preston probe data and pitot probe surveys. The locations of the five instrumentation ports were $S=11.125$, 15.750, 21.750, 27.750, and 33.750 in. (28.26, 40.01, 55.25, 70.49, and 85.73 cm).

The model had a bleed port in the forebody wedge that had a perforated plate [hole size was 0.0165-in. (0.419-mm) diameter with a porosity of 31%] on the top of the forebody and a cover plate on the bottom of the forebody. The cover plate was removed when bleeding off the boundary layer was desired. The bleed plate was 3.8 in. (96.5 mm) long by 15 in. (381 mm) wide, and its leading edge was located 6.1 in. (155 mm) from the leading edge of the model. The boundary-layer bleed was driven by the pressure ratio between the top of the wedge and the bottom of the wedge. This ratio was approximately 2. The bleed rate was measured using a probe similar to the probes described in Ref. 18. The bleed rate for the present tests was 0.12 lb/s/ft^2 (0.59 kg/s/m^2). Normalizing the bleed rate to the mass flux above the forebody wedge gives a value of 0.0152.

In order to assure that the boundary layer developing on the model would be turbulent, or at least have the same attributes for each test run, a boundary-layer trip having repeatable characteristics was used.[19] A trip made from 0.010 in. (0.127 mm) thick aluminum tape (shown in Fig. 2) was placed 2 in. (50.8 mm) from the leading edge of the model. The authors are not aware of any documented use of such a trip design. The philosophy of such a trip is that small vortices result from the triangular leading edges, and these vortices promote transition. The present results indicate that this is true.

Three test conditions were investigated. They were bleed, no bleed, and no bleed with tripping. Comparisons will be made for the various data sets. No LDV data were taken in the duct for the tripped case. The inlet was designed for a freestream

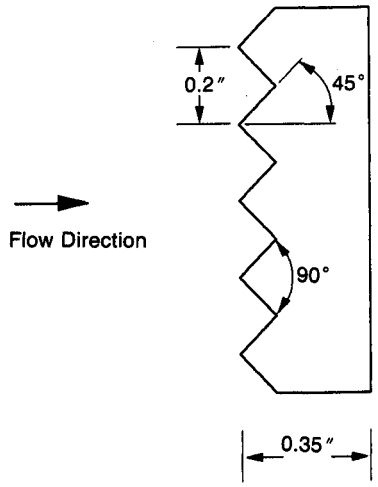

Fig. 2 Boundary-layer trip.

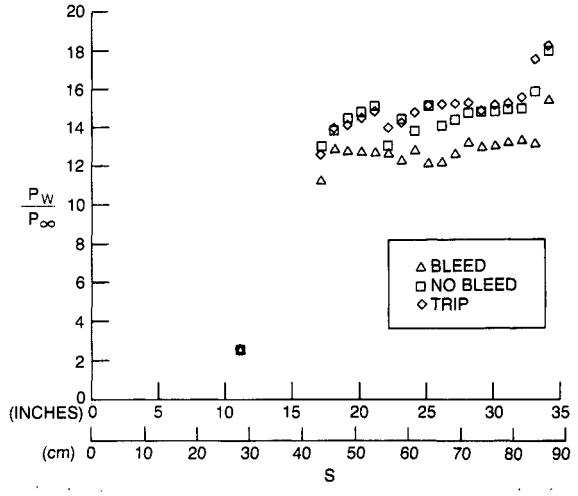

Fig. 3 Wall pressure distributions.

flow of Mach 3, but since only a limited amount of testing could be carried out on this model, it was decided to carry tests out at Mach 4, an off-design condition.

Instrumentation

As previously mentioned, a variety of instrumentation was used to extract the maximum amount of information from the experiment. The primary optical diagnostic instrument was a two-dimensional, two-color, fringe-type LDV system utilizing burst counter type of Doppler processors. This system has been described in Ref. 20. To obtain good statistical ensembles at each measurement point, 2000 samples of both U and V were taken at each point. The aerosol particles used for these tests consisted of polystyrene microspheres (1.09-μ diam).[21] The particles were injected in the wind-tunnel settling chamber approximately 8 ft (2.4 m) ahead of the nozzle throat.

A total of 18 static pressure taps were located along the centerline of the lower wall. The pressures were measured with an electronically scanned pressure (ESP) system that consisted of two modules, each containing 16 pressure transducers. Each transducer was calibrated before a run by drawing a vacuum on the tunnel test cell where the transducers were located and by monitoring the test cell pressure with a reference transducer.

The Preston probe used for the surface shear measurements was a circular stainless tube having an o.d. of 0.052 in. (1.32 mm). Calibrations of this device were obtained from Ref. 22. The Preston probe and the local wall static pressure tap were mounted on a small instrumentation port that could be located at four locations on the upper surface of the duct and one station on the forebody wedge ahead of the inlet cowl. The Preston probe could also be removed from the instrumentation port and mounted at six different locations on the lower wall of the inlet. In this case, the local wall static pressure along the centerline of the lower duct surface was used in conjunction with the Preston probe pressure to compute the wall shear.

The Mach number surveys were made with a miniature pitot traverse that could be placed in each of the five instrumentation ports. The pitot probe was made from stainless steel tubing and was flattened at the tip to a height of 0.041 in. (1.04 mm). Resolution of the traverse was 0.001 in. (0.025 mm). It was assumed that the local static pressure was a constant across the height of the duct at a given axial location. The Mach number was determined from the ratio of the pitot pressure and the local wall static pressure.

Except for a small number of LDV profiles, which were taken off the centerline and which will be discussed later in the paper, all data including pitot, Preston probe, LDV, and wall static pressures were taken on the centerline of the model. There are probably some three-dimensional effects in the duct because the duct does have a finite width-to-height ratio of 4, and there are side wall boundary layers; however, no major effort was made to quantify these effects at this time.

The LHI used in these experiments was a dual plate system and used a pulse ruby laser as the primary light source.[24] There was one major difference in the present setup vs Ref. 24. The pulsed ruby laser was combined with the standard schlieren system used with the tunnel to illuminate a larger field of view in the test section. The new field of view had a diameter of 24 in. (61 cm). Some problems were encountered in matching path lengths between the scene beam and the reference beam but were overcome and resulted in excellent quality holograms. Two separate holograms were recorded (one with flow off, the second with flow on) for each test condition. Reconstruction of the holograms to form interferograms took place in a reconstruction lab after the run was completed. By using the "flow on" hologram only, a shadowgraph reconstruction can be obtained from the same scene for which the interferogram is constructed.

In the holographic interferometer testing phase, only the influences on the optical beam due to the flow inside the duct are of interest. Because the duct was 4 in. (10.16 cm) wide, and the nozzle flow was 16 in. (40.64 cm) wide, a large amount of tunnel freestream flow could pass on either side of the duct and, thus, through the optical beam path. A method was devised by which this freestream flow would not influence the interferometer measurements of the duct flow. This was accomplished by designing some aerodynamically shaped optical tubes that were mounted onto each side of the duct. Each set of tubes was approximately 6 in. (15.2 cm) wide. The combination of the two tubes and the duct spanned the flowfield, and the laser beam passed through the tubes and the duct. Since there was no flow through the tubes, the external flow around the inlet did not influence the interferometer measurements of the flow inside the duct.

Facility Description and Test Conditions

All tests were carried out in the Naval Surface Warfare Center (NAVSWC) supersonic wind tunnel no. 2. Tunnel 2 is a 16 × 16-in. (40.6 × 40.6-cm) cross-sectional horizontal tunnel with an open jet test section capable of operating over a Mach number range of 0.3 to 5 with a supply pressure ranging from 0.5 to 15 atm. The tunnel is equipped with schlieren-quality glass ports that permit a 24-in. (61-cm) diam viewing area. Both intermittent and continuous operation are possible. Air is stored in two interconnected storage systems with a capacity of 1520 ft^3 (43 m^3) at 2700 psia (1.86×10^7 N/m^2) and 937 ft^3 (27 m^3) at 5000 psia (3.445×10^7 N/m^2). Total storage capacity is 39,000 pounds (17,700 kg) of air. The tunnel is equipped with an in-line dryer with reactivation done overnight. A steam heater can yield supply air temperatures from 75 to

225°F (23 to 107°C). For these tests, the tunnel was operated in a continuous mode. The freestream Mach number was 4.00, the supply pressure and temperature were 15 lb/in.^{2} (1.0135×10^5 N/m^2) and 560°R (311 K), respectively, resulting in a unit Reynolds number of 1.3×10^6/ft (4.26×10^6/m).

Results

In Fig. 3, the wall static pressure distributions are shown. One can see the large influence that bleed has on the pressure distribution. The effect of the trip on the wall pressure is not pronounced. It is not obvious that the trip really helped. The turbulence intensities obtained with the LDV give more insight. These are shown in Fig. 4 for the station just prior to the inlet. The turbulence intensities are shown for the tripped and untripped cases, and it can be seen that the turbulence intensities are higher for the tripped case. The turbulence intensities for the untripped case, however, are typical of turbulent boundary layers. Thus, one is left with the uncertainty of whether the trip actually promoted transition or just increased the turbulence level. The boundary layer is approximately 5% thicker for the tripped case.

During the experiment, oil flow studies were carried out in the entrance region of the inlet. These studies indicated that the boundary layer was separated just in front of the inlet. This separation zone extended up to the front of the first port when there was no bleed. When bleed was applied, there was still some separation, but the zone was approximately one-half the size of the unbled zone. Extensive LDV surveys in this area could not detect any flow reversal, thus, indicating a very thin separated layer. From Fig. 3, the pressure ratio of the duct pressure (near the throat region) to the wedge pressure is about 4.5 to 5.5. This is about a factor of 2 greater than would be expected from just the oblique shock from the cowl leading edge. The boundary layer that entered the inlet probably was not able to keep from separating with this magnitude of pressure rise. For an oblique shock to separate the boundary layer for the present conditions, Ref. 23 indicates that a maximum pressure rise of about 5.5–6.0 is needed. Thus, the effects of the cowl shock coupled with the shocks from the side walls and the pressure rise across the waves from the compression surface may all combine to promote boundary-layer separation in the inlet entrance.

It should be pointed out that there is a very rapid rise in pressure in the last couple of pressure stations. It is believed that this was caused by flow separation at the end of the duct. This results because the duct flow empties into the base region of the model, and separation occurs near the trailing edge of the duct. The last pressure tap was only 0.6 in. (15 mm) from the trailing edge; thus, the pressures at these last taps were being influenced by the separation.

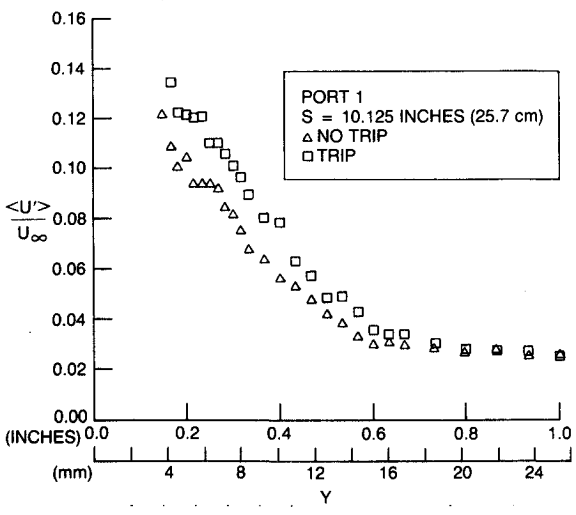

Fig. 4 Turbulence intensities.

The Mach number profiles taken at the five locations on the model are shown in Fig. 5. The Mach number was determined from the ratio of the pitot pressure and the local wall static pressure. It was assumed that the static pressure was constant across the height of the duct. This may lead to some errors in the Mach number near the throat where it is expected that the static pressure is not constant across the height of the duct. The inviscid design value of the Mach number entering the duct should be 2.36. This agrees well with the Mach number determined for the bleed case.

A more meaningful way to show the data is to plot the total pressure (pitot pressure) referenced to the supply pressure. These results are shown in Fig. 6. These results also give an indication of the pressure recovery that the inlet provides. At a Mach number of 4, the normal shock recovery (pitot pressure/supply pressure) is 0.1388; thus, one would anticipate that the measured values inside the inlet would be greater than 0.1388. At the 10.125-in. station, the Mach number profiles show that the boundary layer was approximately 0.2 in. (5 mm) thick. There is a slight overshoot in the Mach number near the boundary-layer edge, and this is prevalent for all three cases. The position $y = 0$ was located on the lower surface, and measurements were made away from the lower surface.

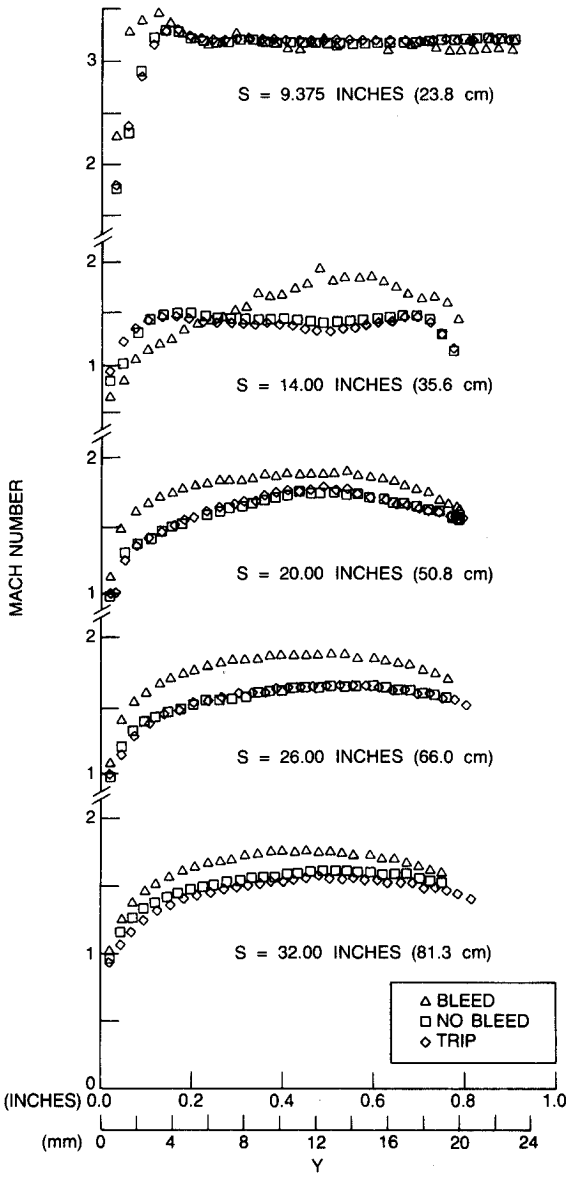

Fig. 5 Mach number distributions.

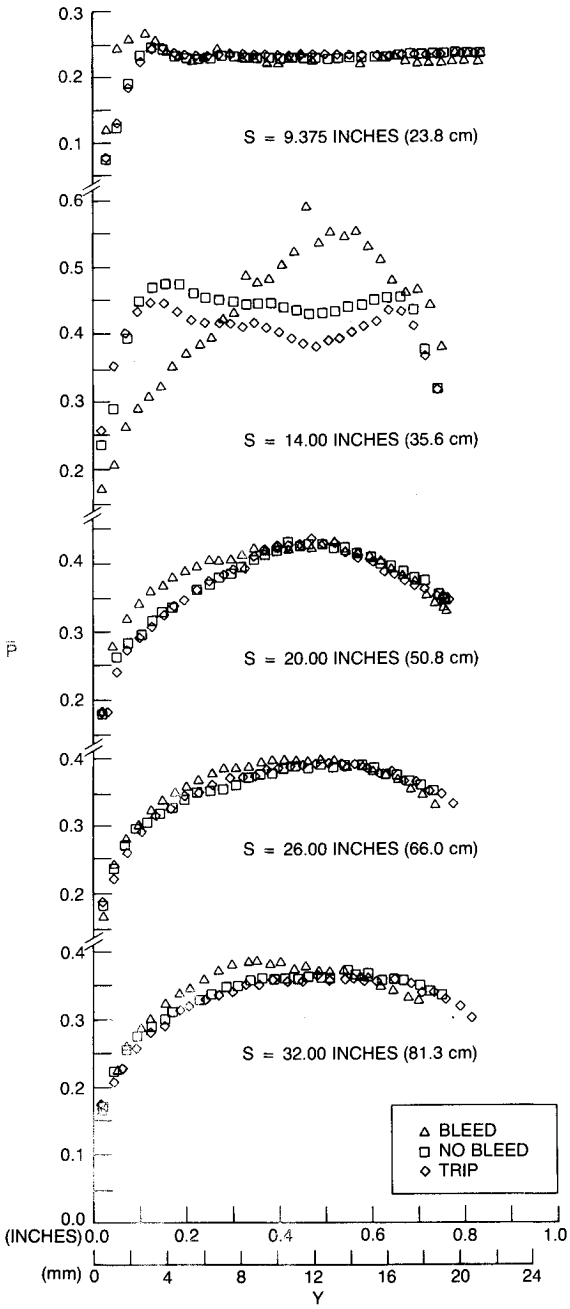

Fig. 6 Pitot profiles.

At the next station, the Mach number profiles are very different between the bleed and no-bleed test conditions. It appears that the no-bleed case is more uniform, but the pressure recovery is higher for the bleed case. This would be expected since the low energy flow has been removed. The flow in this region was very complex. This is because the cowl shock, the waves from the compression surface, the expansion waves from the lower surface, and the separated boundary layer are all combining in this region to give a very nonuniform flow. By the time the flow arrives at the third station, the flow begins to become more uniform. There is almost no difference between the tripped and untripped (no suction) cases.

Some of the velocity profiles obtained are shown in Fig. 7 for a series of locations through the inlet. Again the data are shown for both bleed and no-bleed. It should be noted that these stations are different from the Mach number surveys, and no LDV data were taken with a trip. These velocity profiles reflect the substantial effect that bleeding off the entrance boundary layer had on the velocity profiles within the duct. The LDV measurements shown in Fig. 7 for $S = 15.45$ in. (39.2 cm) were made through the small forward window, thus limiting the field of view of the flowfield.

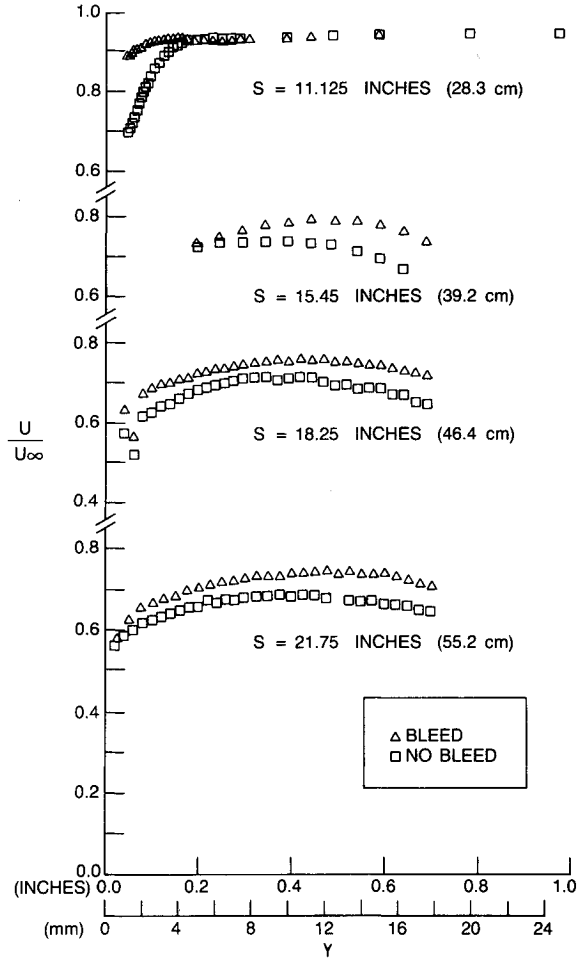

Fig. 7 Velocity profiles.

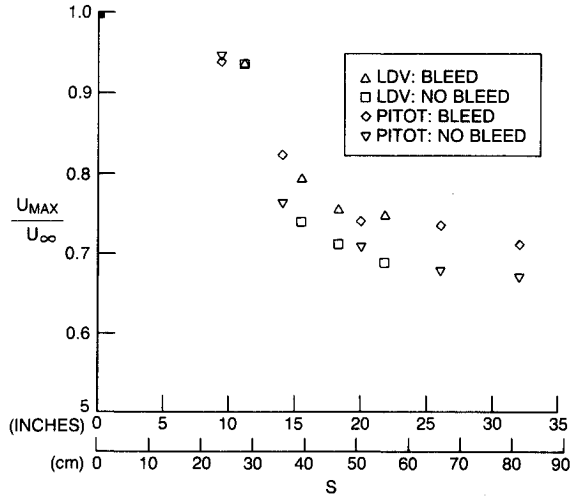

Fig. 8 Maximum velocity distributions through inlet.

In Fig. 8 the velocity is shown as a function of position along the duct. The velocity shown is the maximum at that particular location as determined from both the LDV and the Mach number surveys. In the determination of the velocity from the Mach number, it was assumed that the flow was adiabatic through the duct. It is seen that the agreement between the LDV and pitot measurements is very good.

Shown in Fig. 9 are velocity surveys for the centerline and 1 in. (2.54 cm) on either side of centerline. These were taken at $S = 21.75$ in. (55.2 cm) for both bleed (Fig. 9a) and no-bleed

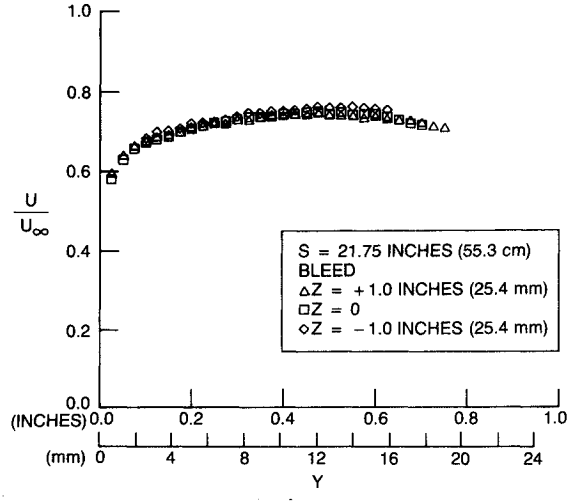

Fig. 9a Velocity profiles off centerline (bleed).

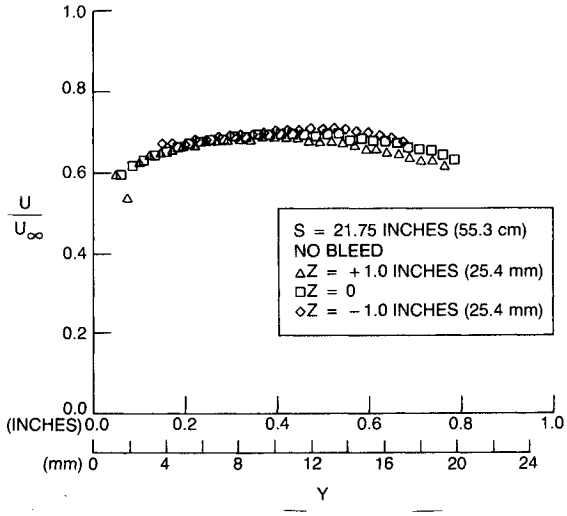

Fig. 9b Velocity profiles off centerline (no bleed).

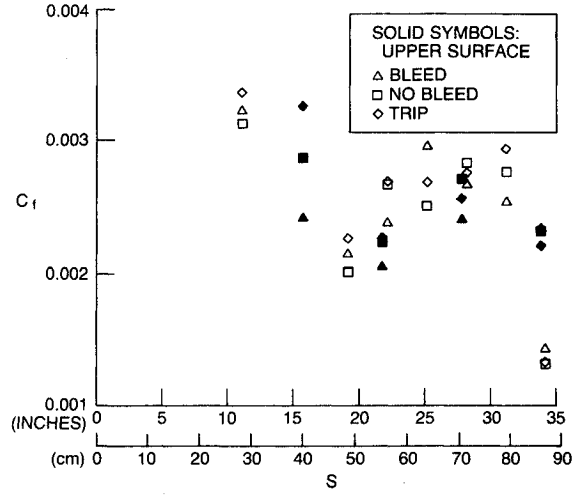

Fig. 10 Skin friction coefficient distribution.

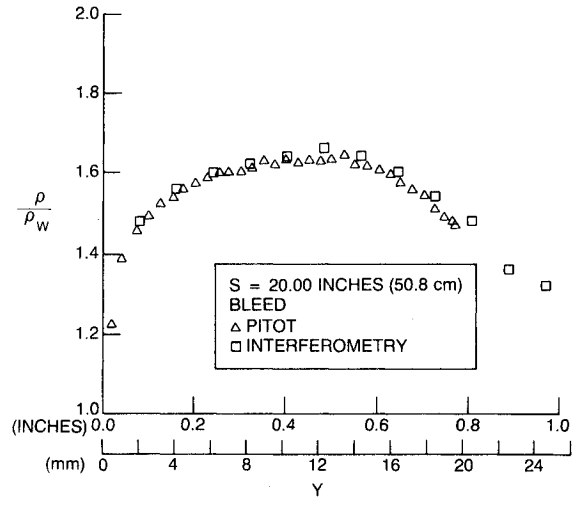

Fig. 11 Density distributions.

(Fig. 9b) conditions. There appears to be a slight asymmetry for both cases. For the no-bleed case, the maximum difference between the two outside profiles is about 5%, whereas for the bleed case, the maximum difference is about 3%. There are probably several reasons for this, but it is surmised that the separated flow in the entrance region is probably the major cause for this asymmetry since surface oil flow visualization indicated an asymmetrical separation.

As was mentioned previously, the local surface shear was determined from the Preston probe using the correlation of Ref. 22. Shown in Fig. 10 are the values for the skin friction that were determined from the Preston probe data. The skin-friction coefficient was determined from the local shear stress by using the equation

$$c_f = 2\,\tau_w/\rho U^2 = 2\tau_w/\gamma P_w M_{cl}^2$$

where γ is the ratio of specific heats, P_w is the local wall pressure, and M_{cl} is the local centerline Mach number at the location where the shear was measured. It should be re-emphasized that the surface distance S is measured on the surface of the wedge and the lower surface of the duct and is measured from the leading edge of the wedge. Thus, the cowl is at $S = 11$ in. (27.9 cm), and all locations for measurements on the upper surface of the duct are measured relative to the model's leading edge. We do not see as much influence of bleed on the skin friction, probably because of the boundary layer's quick response to local conditions. The boundary layer, in effect, does not have a long memory of what happened on the wedge once it gets into the inlet. In fact, the values for the skin friction for both the upper and lower surfaces of the duct have about the same values, even though the boundary layer on the lower surface has had a much longer distance to develop. The values of skin friction on the upper surface are somewhat smaller than the lower surface, which is surprising. One would have expected that since the length Reynolds number is larger for the lower surface, the friction coefficient would have been lower for the data without bleed. The skin friction values at the end of the duct may be suspect because of separation at this location.

The interferometric data were reduced using a similar method as described in Ref. 25. For comparison, the density was computed from the Mach number profiles. Again it was assumed that the flow was adiabatic and by using the Crocco solution, a density profile may be computed. These results are shown in Fig. 11 for one test condition, and it can be seen that there is very good agreement. A comprehensive data analysis was carried out for the interferometric measurements and is described in Ref. 26.

Conclusions

A series of tests have been carried out on a generic scramjet inlet with 33 deg of turning at a Mach number of 4. Measurements include two-dimensional LDV measurements of mean and fluctuating velocity profiles, Mach number surveys, static pressure distributions, and wall-shear stress distributions along the inlet centerline. Also, density distributions were obtained from LHI. Measurements include the effects due to

total boundary-layer ingestion into the inlet and also results where the boundary layer has been bled off prior to entering the inlet. In addition, a boundary-layer trip was used for selected cases. Some conclusions are as follows:

1) The trip did promote higher turbulence levels in the boundary layer, but this effect was not a major factor of the inlet's performance for these conditions.

2) Boundary-layer bleed was effective in decreasing the separation region near the inlet throat, resulting in an increase in the pressure recovery in the duct. This effect persisted through the entire duct length.

3) The effect of bleed on skin friction does not appear to be as persistent. It appears that the wall shear is much more responsive to local flow conditions and that the upstream history is quickly washed out.

Acknowledgments

This work was supported by Naval Surface Warfare Center Independent Research Task Area RR02302. The authors wish to acknowledge the work of John Gibson, U.S. Navy, who helped perform the calculations for the design; Armand L. Ratte, who designed the model; Timothy Smith for the measurements of the bleed flow rate; Jay Marshall and Ralph Truitt for the efficient operation of the wind-tunnel facility; and James Keirsey and members of his staff at the Applied Physics Laboratory for many helpful discussions.

References

[1]Waltrup, P. J., "Liquid Fueled Supersonic Combustion Ramjets: A Research Perspective of the Past, Present and Future," AIAA Paper 86-0158, Jan. 1986.

[2]Dillon, J. L., Marcum, D. C., Jr., Johnston, P. J., and Hunt, J. L., "Aerodynamic and Inlet Flow Characteristics of Several Hypersonic Airbreathing Missile Concepts," *Journal of Aircraft*, Vol. 18, No. 4, 1981, p. 231.

[3]Hunt, J. L., Johnston, P. J., Cubbage, J. M., and Dillon, J. L., "Hypersonic Airbreathing Missile Concepts Under Study at Langley," AIAA Paper 82-0316, Jan. 1982.

[4]Hunt, J. L., Johnston, P. J., and Riebe, G. D., "Flow Fields and Aerodynamic Characteristics for Hypersonic Missiles with Mid-Fuselage Inlets," AIAA Paper 83-0542, Jan. 1983.

[5]Johnston, P. J., and Hunt, J. L., "Mach 6 Flow-Field and Boundary Layer Surveys Beneath the Forebody of an Airbreathing Missile," AIAA Paper 84-0233, Jan. 1984.

[6]Dunsworth, L. C., and Reed, G. J., "Ramjet Engine Testing and Simulation Techniques," *Journal of Spacecraft and Rockets*, Vol. 16, No. 6, 1979, pp. 382–388.

[7]McLafferty, G. H., Krasnoff, E. L., Ranard, E. D., Rose, W. G., and Verara, R. D., "Investigation of Turbulent Inlet Design Parameters," United Aircraft Corp., East Hartford, CT, Rept. R-0790-13, Dec. 1955.

[8]Om, D., and Childs, M. E., "An Experimental Investigation of Multiple Shock Wave/Turbulent Boundary Layer Interactions in a Circular Duct," AIAA Paper 83-1744, July 1983.

[9]Gessner, F. B., Ferguson, S. D., and Lo, C. H., "Experiments on Supersonic Turbulent Flow Development in a Square Duct," *AIAA Journal*, Vol. 25, No. 5, 1987, pp. 690–697.

[10]Sajben, M., Bogar, T. J., Kroutil, J. C., and Salmon, J. T., "Factors Influencing Velocity Distributions at Inlet/Combustor Interfaces," Chemical Propulsion Information Agency, Laurel, MD, CPIA Pub. 347, Vol. 3, 1981, pp. 321–331.

[11]Bogar, T. J., Sajben, M., and Kroutil, J. C., "Characteristic Frequency and Length Scales in Transonic Diffuser Flow Oscillations," AIAA Paper 81-1291, June 1981.

[12]Sajben, M., Bogar, T. J., and Kroutil, J. C., "Forced Oscillation Experiments in Supercritical Diffuser Flows with Applications to Ramjet Instabilities," AIAA Paper 81-1487, July 1981.

[13]Paynter, G. C., and Chen, H. C., "Progress Toward the Analysis of Supersonic Inlet Flows," AIAA Paper 83-1371, June 1983.

[14]Dunsworth, L. C., and Woodgrift, K. E., "Dual Mode Scramjet, Part I: Inlet Design and Performance Characteristics," The Marquardt Corp., Van Nuys, CA, AFAPLTR-67-132, Part I, Dec. 1967.

[15]Trexler, C. A., "Inlet Performance of the Integrated Langley Scramjet Module (Mach 2.4 to 7.6)," AIAA Paper 75-1212, Sept.-Oct. 1975.

[16]Hsieh, T., Wardlaw, A. B., and Collins, P., "Numerical Investigation Of Unsteady Inlet Flow Fields," AIAA Paper 84-0031, Jan. 1984.

[17]Shapiro, A. H., *The Dynamics and Thermodynamics of Compressible Fluid Flow*, Vol. I, Ronald Press, New York, 1953.

[18]Smith, T. S., "Theory and Experimental Verification of Compressible Low Density Subsonic Flow Through Curved Porous Surfaces with Non-uniform Thicknesses," AIAA Paper 87-1387, June 1987.

[19]Rose, W. C., private communication, Dec. 1986.

[20]Yanta, W. J., and Ausherman, D. W., "A 3-D Laser Doppler Velocimeter for Use in High Speed Flows," 7th Biennial Symposium on Turbulence, Univ. of Missouri-Rolla, Rolla, MO, Sept. 21–23, 1981.

[21]Bangs, L. B., *Uniform Latex Particles*, Seradyn Inc., Indianapolis, IN.

[22]Yanta, W. J., Brott, D. L., and Lee, R. E., "An Experimental Investigation of the Preston Probe Including Effects of Heat Transfer, Compressibility and Favorable Pressure Gradient," AIAA Paper 69-648, June 1969.

[23]Kuehn, D. M., "Experimental Investigation of the Pressure Rise Required for the Incipient Separation of Turbulent Boundary Layers in Two-Dimensional Supersonic Flow," NASA Memo. 1-21-59a, Feb. 1959.

[24]Hannah, B. W., and Havener, A. G., "Applications of Automated Holographic Interferometry," *Proceedings of the International Congress on Instrumentation in Aerospace Simulation Facilities*, IEEE, Piscataway, NJ, 75-CH0993-GAES, 1975, pp. 237–246.

[25]Bachalo, W. D., and Houser, M. J., "Optical Interferometry in Fluid Dynamics Research," *Automated Reduction of Data from Images and Holograms,"* NASA CP-2477, Jan. 1985.

[26]McArthur, J. C., Yanta, W. J., Spring, W. C., and Gross, K. U., "Laser Holographic Interferometric Measurements of the Flow in a Scramjet Inlet at Mach 4," AIAA Paper 89-0043, Jan. 1989.